1 Results of Simulations

The results of the numerical simulations will be presented and discussed in this chapter. First for the qubit state evolution and then for the cat code encoding.

1.1 Qubit State Control

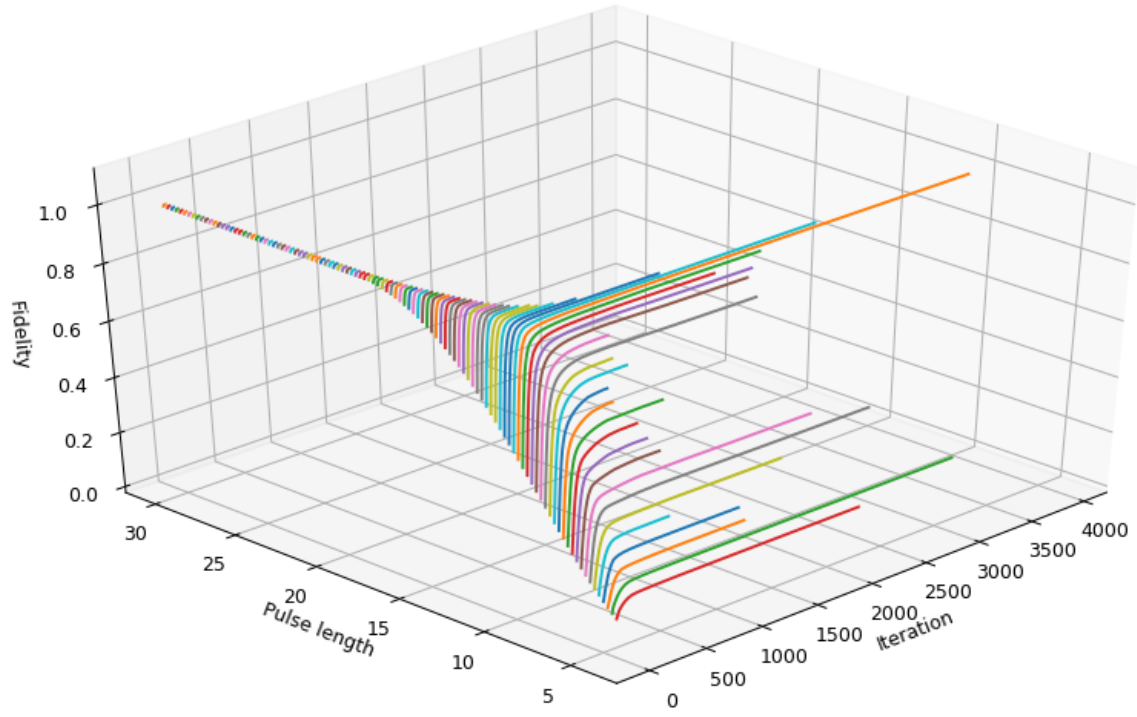

Figure 1.1: Fidelity during optimizations for every pulse length (ns). The different colors help distinguish the lines.

1.1.1 $|0\rangle \rightarrow |1\rangle$ state evolution

In Figure 1.1 the fidelity during all optimizations (with pulse lengths from 4.25 ns to 30 ns) are plotted. The "starting fidelity" is the fidelity which is obtained with the guess pulses while the "optimized fidelity" is the fiedlity obtained with the optimized pulses. For pulse lengths longer than 15 ns the fidelity starts at values close to the goal ($F > 0.9$) and the number of iterations is relatively low (less than 85 iterations). In contrast, pulses shorter than 15 ns start at lower fidelities while the number of iterations are roughly one order of magnitude larger with no clear pattern with respect to the pulse length.

To give a more detailed picture, the starting fidelity and optimized fidelity are plotted over pulse length in Figure 1.2. The optimizations where the fidelity goal was not reached, pulse lengths equal to and below 10.50 ns, are marked with stars.

Further analysis is done on pulses with lengths 4.25 ns, 6.0 ns, 8.0 ns, 10.0 ns, 20.0 ns and 30.0 ns. The optimized pulse shapes $\mathrm{Re}(\Omega)$ and $\mathrm{Im}(\Omega)$ are plotted in Figure 1.3 together with the guess pulses. Pulses longer than 20 ns require only fine adjustments to the Blackman guess pulse while shorter pulses have an imaginary part which is maximized for the whole duration of the pulse. In order to gain insight into the shape of the pulse solution, we analyse its spectral content by performing a Fourier analysis.

The spectrum of the control pulse $\Omega(t)$ in the lab frame ($\Omega(t)e^{i\omega_q t}$) is shown in Figure 1.4. For all pulse lengths there is a peak centered roughly at ω_q with a quickly decaying end in positive direction (towards $\omega_q + K_q$). Following the trend, it can be observed that the width of the peak becomes narrower for longer pulses. For the highest pulse length 30 ns there is almost no support at $\omega_q + K_q$ nor $\omega_q - K_q$.

The time evolution of the system under the optimized pulses are visualized by plotting the occupation of the states over time, Figure 1.5, and the projection of the state on the Bloch sphere over time, Figure 1.6.

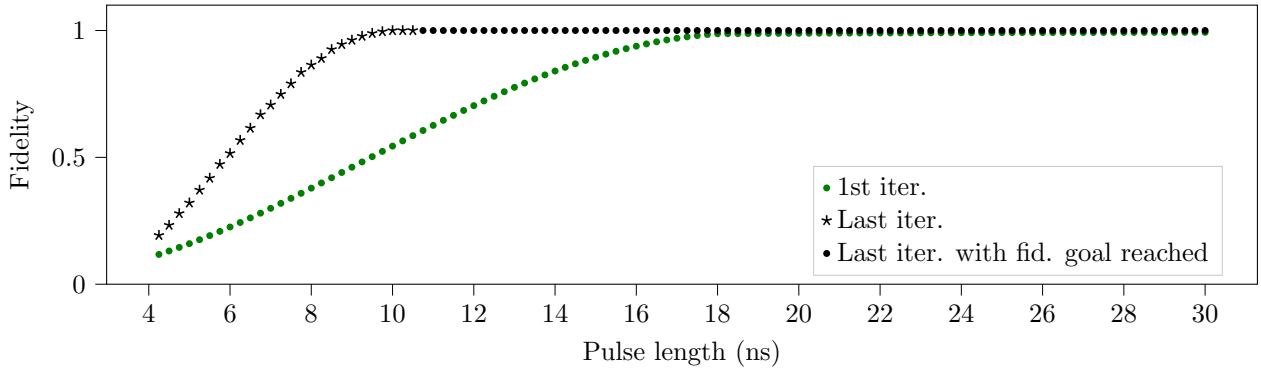

Figure 1.2: Starting fidelity (green) and optimized fidelity (black) of pulse lengths from 4.25 ns to 30 ns.

For short pulse lengths there is not enough time for the evolution from $|0\rangle$ to $|1\rangle$, but for a pulse length of roughly 10.0 ns the goal is reached. Figure 1.5 **(b)** shows a little rise in occupation of $|2\rangle$ around 7.5 ns. From the Bloch sphere visualization it appears that shorter pulse lengths lead to deviations from the pure y-axis rotation. This can be clearly seen in Figure 1.6 **(d)** for a pulse length of 10 ns, where the fidelity goal was reached but short enough that the maximum amplitude is reached for the guess pulse.

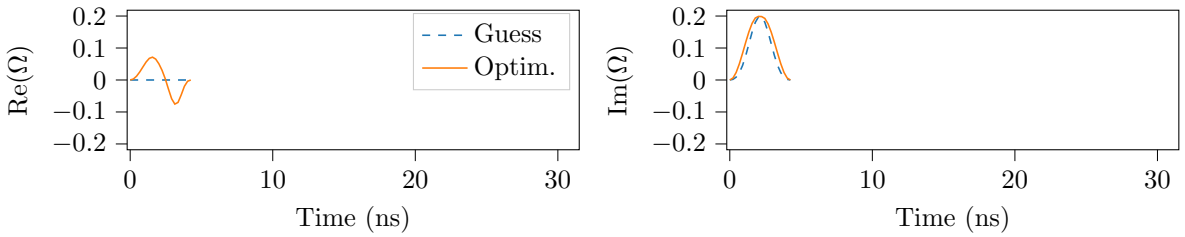

(a) Pulse length 4.25 ns

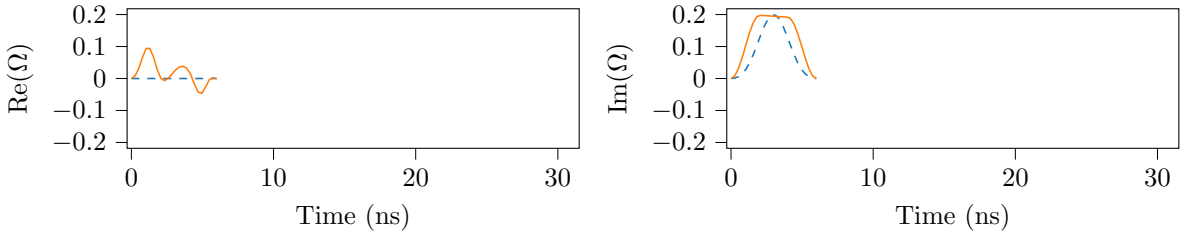

(b) Pulse length 6.0 ns

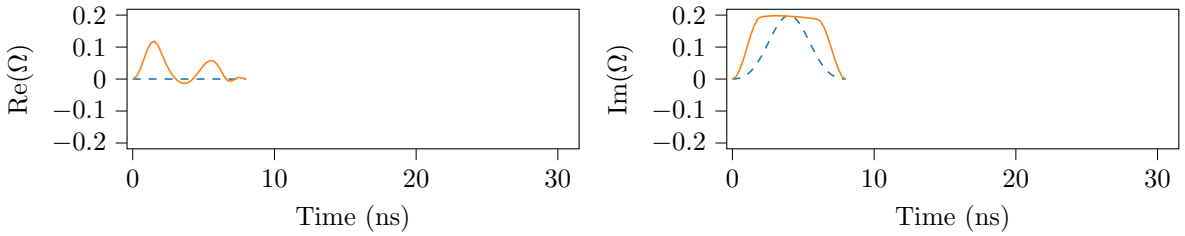

(c) Pulse length 8.0 ns

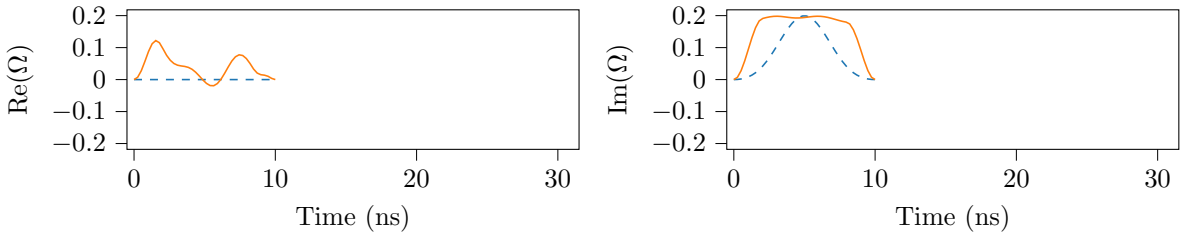

(d) Pulse length 10.0 ns

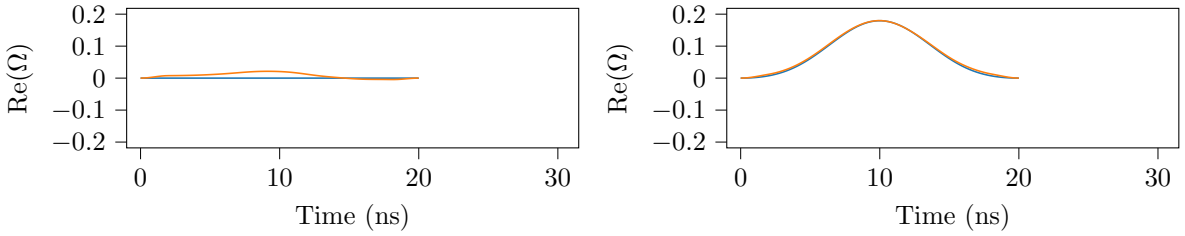

(e) Pulse length 20.0 ns

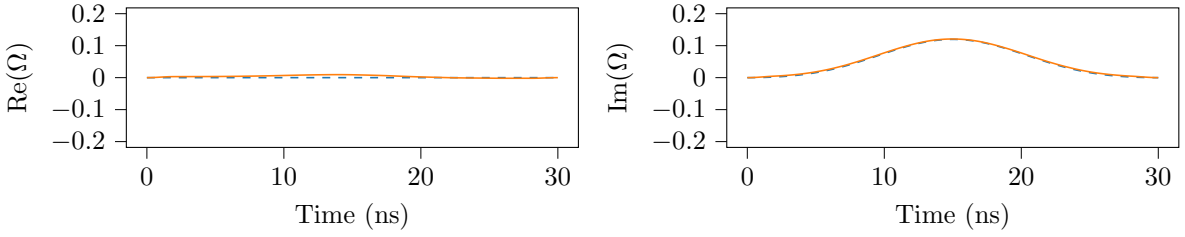

(f) Pulse length 30.0 ns

Figure 1.3: Optimised pulse shapes and guess pulses (dashed) for pulse lengths **(a)** 4.25 ns, **(b)** 6.0 ns, **(c)** 8.0 ns, **(d)** 10.0 ns, **(e)** 20.0 ns, and **(f)** 30.0 ns. Short pulses (<10 ns) change substantially from the starting Blackman shape while long pulses (>20 ns) only require fine adjustments.

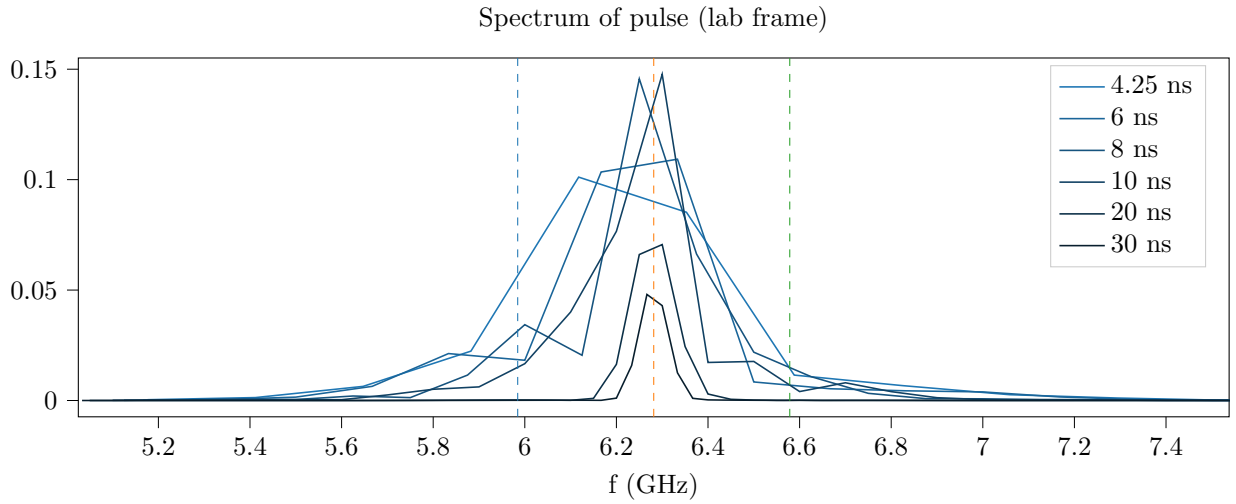

Figure 1.4: Frequency spectrum of the complex pulses in Figure 1.3. The vertical lines indicate (from left to right) $\omega_q - K_q$, ω_q, $\omega_q + K_q$ (all divided by 2π).

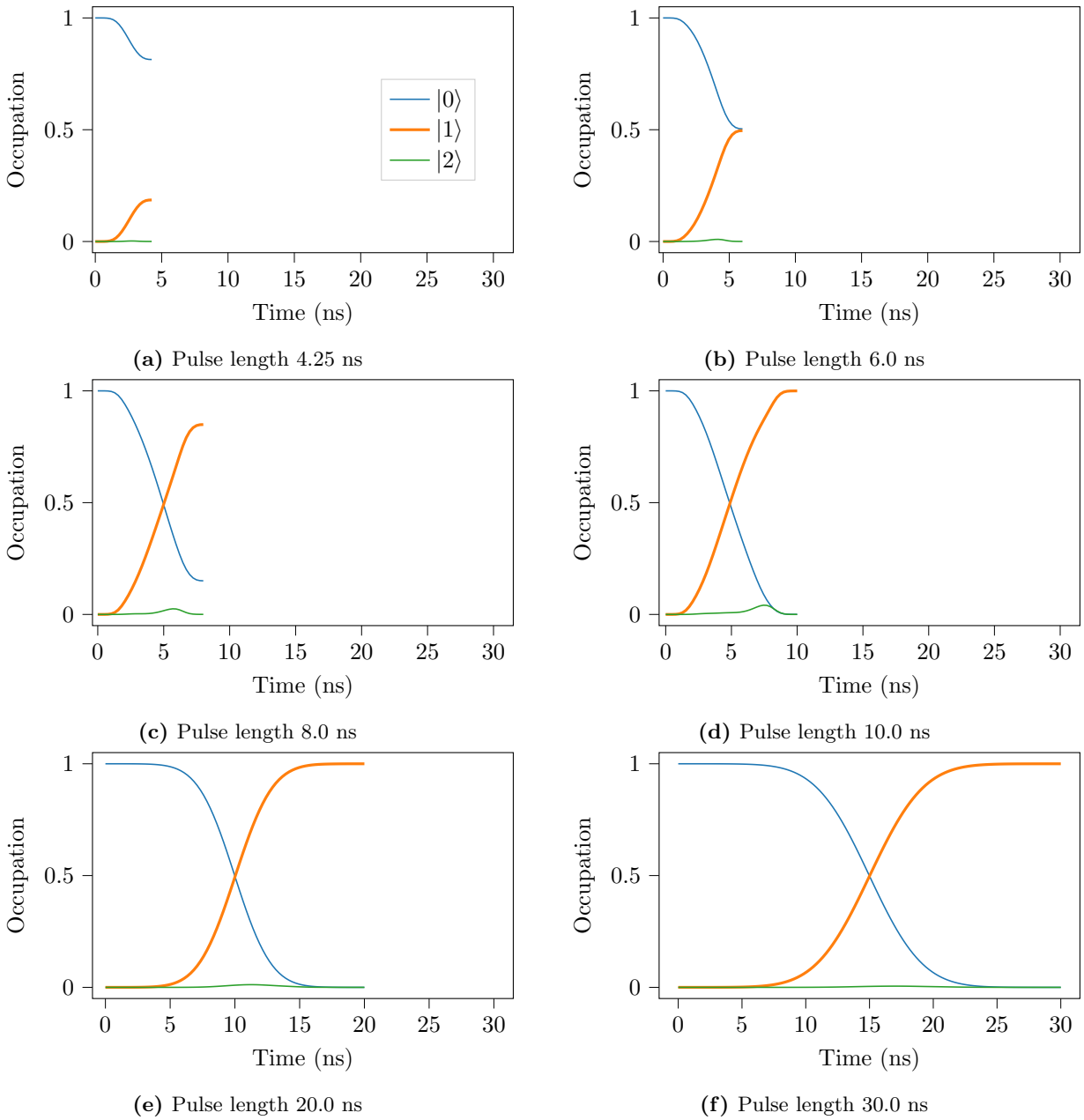

(a) Pulse length 4.25 ns

(b) Pulse length 6.0 ns

(c) Pulse length 8.0 ns

(d) Pulse length 10.0 ns

(e) Pulse length 20.0 ns

(f) Pulse length 30.0 ns

Figure 1.5: Energy level occupation over time during the $|0\rangle \rightarrow |1\rangle$ evolution for different lengths of optimized pulses.

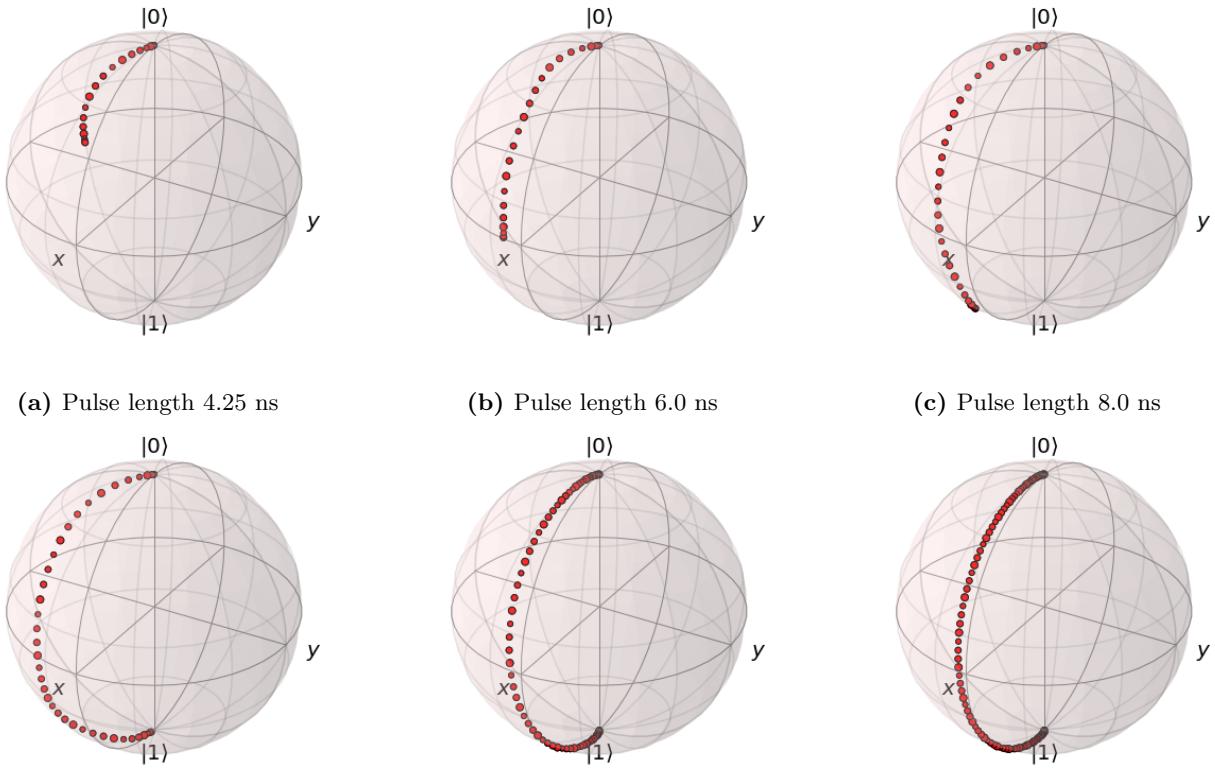

(a) Pulse length 4.25 ns **(b)** Pulse length 6.0 ns **(c)** Pulse length 8.0 ns

(d) Pulse length 10.0 ns **(e)** Pulse length 20.0 ns **(f)** Pulse length 30.0 ns

Figure 1.6: Time dynamics on the Bloch sphere for different lengths of optimized pulses.

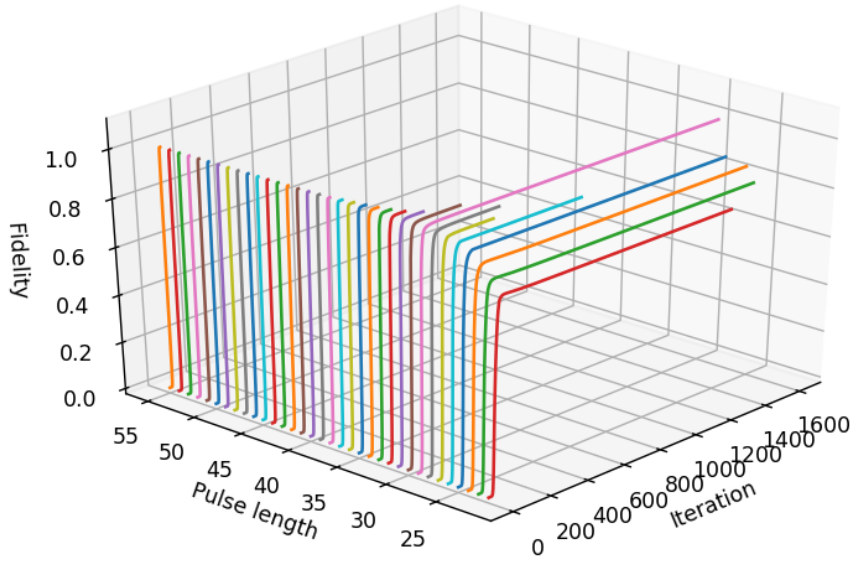

Figure 1.7: Fidelity during optimizations for every pulse length (ns).

1.1.2 $|0\rangle \rightarrow |2\rangle$ state transfer

Once again all optimization runs are shown in Figure 1.7. All runs start at almost zero fidelity while pulse lengths longer than 30 ns reach the fidelity goal of $F > 0.99999$. The number of iterations is relatively low for pulses longer than 30 ns while for shorter pulses the iterations fluctuate. Note that for pulse lengths shorter than 22 ns the optimization stopped after the first iteration due to $\Delta F < 10^{-9}$, therefore those results have been ommitted.

In Figure 1.8 the fidelity is shown with respect to the pulse length and it is seen that the fidelity goal is reached for pulses longer than and including 30 ns.

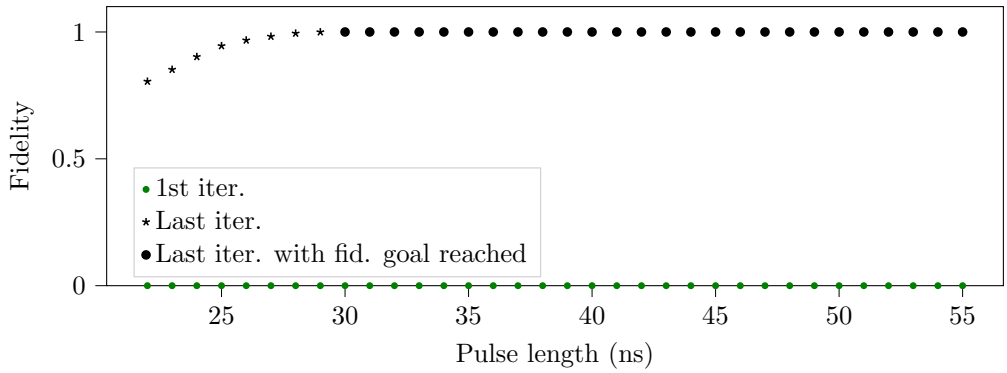

Figure 1.8: Starting fidelity (green) and optimized fidelity (black) of pulse lengths from 22 ns to 55 ns.

The optimized pulses are shown in Figure 1.9. For all pulse lengths the pulses have roughly the same shape, with a quick rise and a short plateau, then oscillations until the end. The longest pulse at 55 ns has more oscillations than shorter ones, but instead they are lower in amplitude. To get some insight, the frequency spectrum, Figure 1.10, shows large support at ω_q and $\omega_q + K_q$. For longer pulses, the peak at $\omega_q - K_q$ disappears. Just as the previous state evolution, the peaks narrow for longer pulse lengths.

The occupation dynamics in Figure 1.11 show a slow oscillation for all pulse lengths for all states. Further, the occupation probability of $|1\rangle$ rises to about 0.75 until the middle-point of the pulse and then falls to zero in the end, while $|2\rangle$ starts to rise at the point of the population inversion. For the shorter pulse lengths it can be seen that there isn't enough time to realise the evolution.

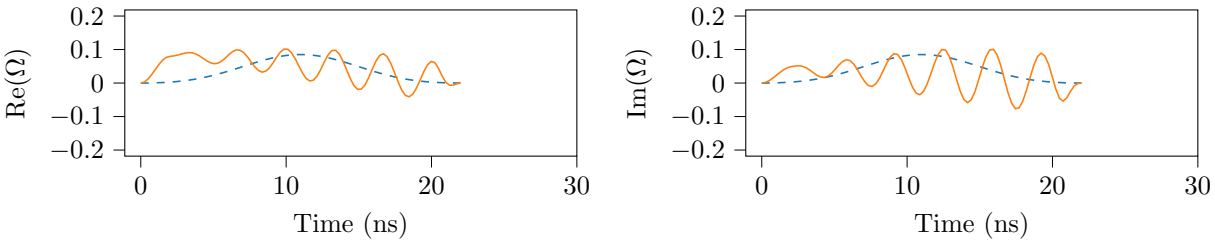

(a) Pulse length 22.0 ns

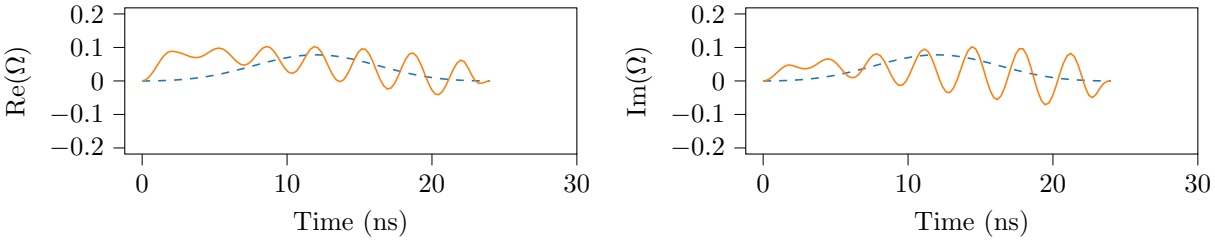

(b) Pulse length 24.0 ns

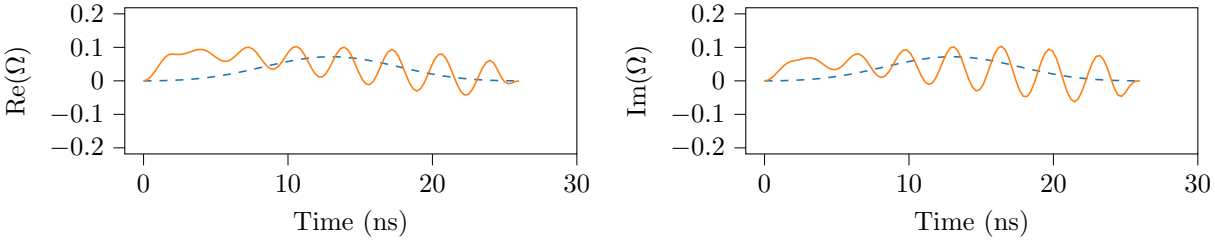

(c) Pulse length 26.0 ns

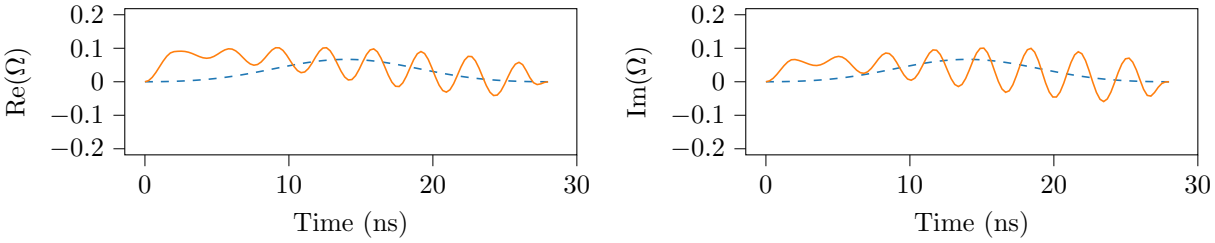

(d) Pulse length 28.0 ns

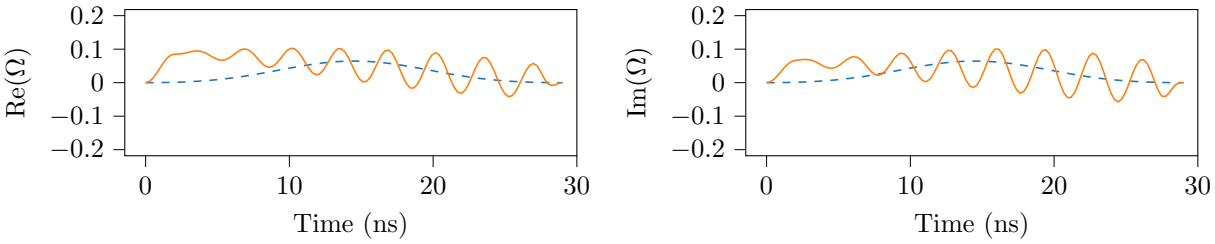

(e) Pulse length 29.0 ns

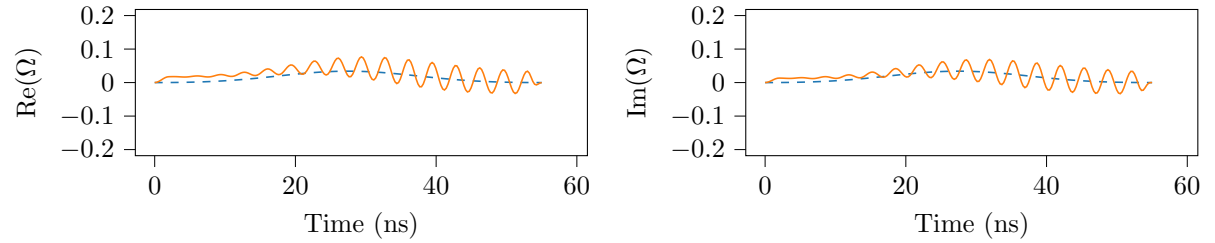

(f) Pulse length 55.0 ns

Figure 1.9: Optimised pulse shapes and guess pulses (dashed) for pulse lengths **(a)** 22 ns, **(b)** 24 ns, **(c)** 26 ns, **(d)** 28 ns, **(e)** 29 ns, and **(f)** 55 ns. Oscillations appear in all solutions.

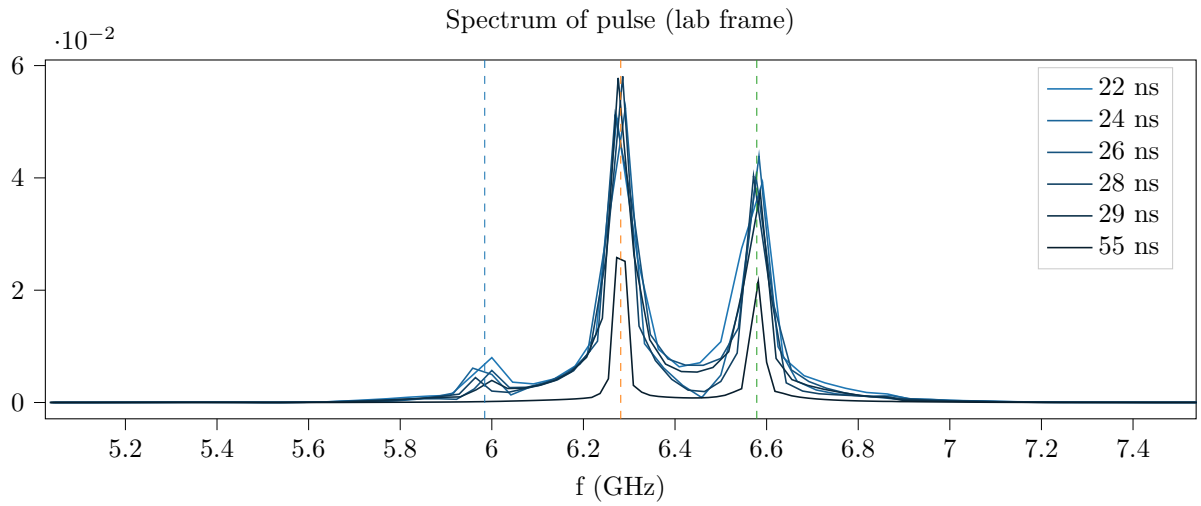

Figure 1.10: Frequency spectrum of the complex pulses in Figure 1.9. The vertical lines indicate (from left to right) $\omega_q - K_q$, ω_q, $\omega_q + K_q$ (all divided by 2π).

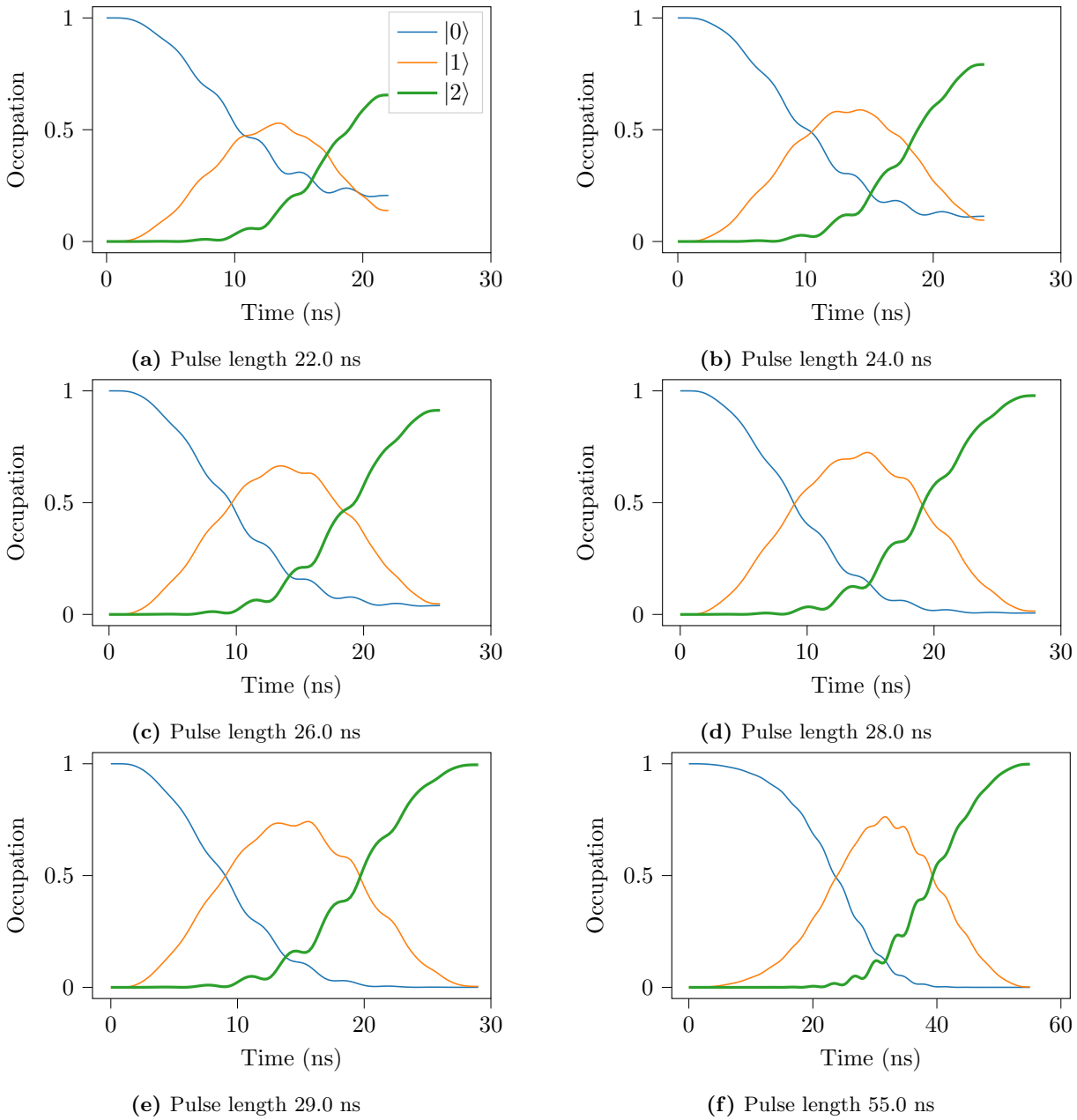

(a) Pulse length 22.0 ns

(b) Pulse length 24.0 ns

(c) Pulse length 26.0 ns

(d) Pulse length 28.0 ns

(e) Pulse length 29.0 ns

(f) Pulse length 55.0 ns

Figure 1.11: Energy level occupation over time during the $|0\rangle \rightarrow |2\rangle$ evolution for different lengths of optimized pulses.

1.2 Cat Code Encoding

The cat encoding optimization reached the convergence criteria of $\Delta F < 10^{-6}$ after 2389 iterations (totalling at roughly 41 hours and 28 minutes) with a fidelity $F = 0.999234$, (recall the fidelity measure for multiple objectives in **??**). The individual fidelities for the 6 initial states are shown in Table 1.1, where we can see that all individual fidelities are above 0.999000.

Table 1.1: Fidelities for the individual state transfers (ordered from highest to lowest).

State	F
$(\|0\rangle + i\,\|1\rangle)/\sqrt{2}$	0.99939453
$(\|0\rangle - \|1\rangle)/\sqrt{2}$	0.99932348
$(\|0\rangle + \|1\rangle)/\sqrt{2}$	0.99930147
$\|0\rangle$	0.99920509
$\|1\rangle$	0.99918837
$(\|0\rangle - i\,\|1\rangle)/\sqrt{2}$	0.99899637

Further to see how well the qubit was mapped to the cat code basis, multiple states spread around the Bloch sphere were transferred with the pulse. The corresponding fidelities are shown on the Bloch sphere in Figure 1.12 where we can se an asymmetry with larger fidelities toward $(|0\rangle + i\,|1\rangle)/\sqrt{2}$. All in all the minimum fidelity of any of the states is 0.998996.

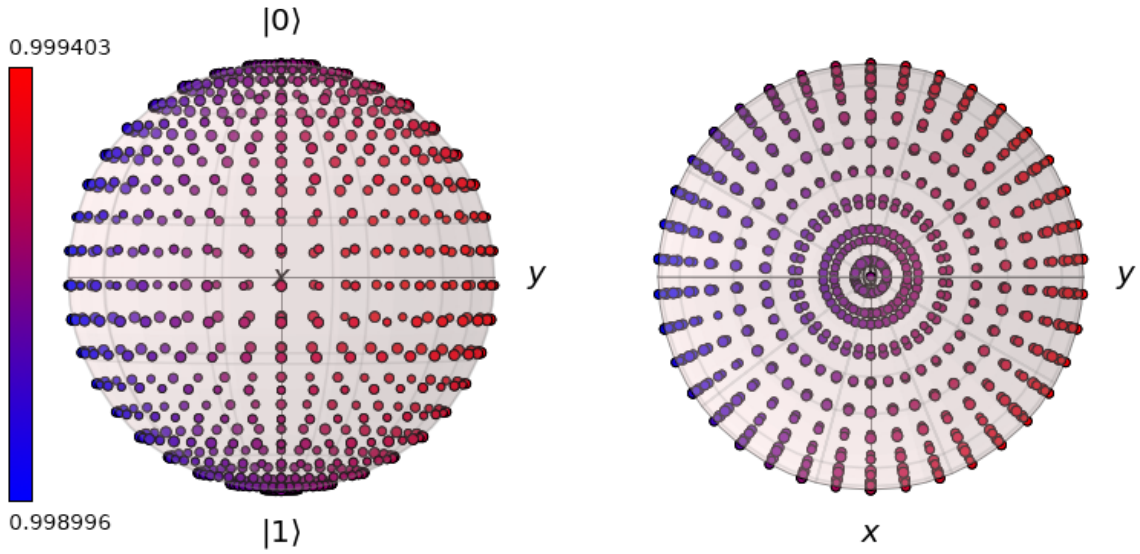

(a) Side view of Bloch sphere.

(b) Top view of Bloch sphere.

Figure 1.12: The fidelities of many simulated state transfers shown on the Bloch sphere. There is an asymmetry in the fidelity with higher fidelity towards the state $(|0\rangle + i\,|1\rangle)/\sqrt{2}$.

The pulse shapes of the qubit and resonator are shown in Figure 1.13. Comparing the resonator and qubit we can see that the resonator pulse has rapid oscillations throughout the whole pulse while the qubit exhibits some small quick oscillation at sparse times. The spectrum of the pulse is shown in **??** and gives us some insight into the pulse shapes. The qubit control pulse shows a wide peak at ω_q, two small peaks at ω_r and $2\omega_r - \omega_q$ and two barely noticable peaks at $\frac{1}{4}\omega_r$ and $\frac{1}{2}\omega_r$. The resonator pulse has one wide peak at ω_r, a smaller one at ω_q and an even smaller peak at $2\omega_r - \omega_q$.

The dynamics of the qubit is shown in Figure 1.15 for all state transfers. Here we see that there is always a rapid oscillation present in the occupation probability. Looking at the dynamical behaviour one can see that common for all transfers is for the qubit to stay somewhat close to an equal superposition between $|0\rangle$ and $|1\rangle$ and then at circa 50 ns evolve to $|0\rangle$.

One interesting measure we can look at is the maximum occupation of the 8 resonator states. This can give

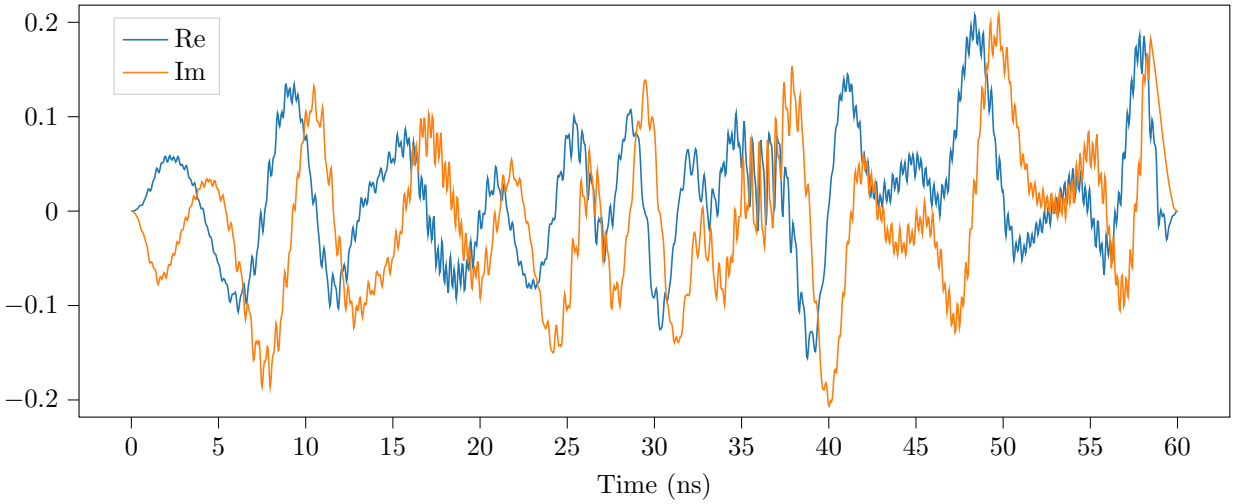

(a) Qubit control pulse shape.

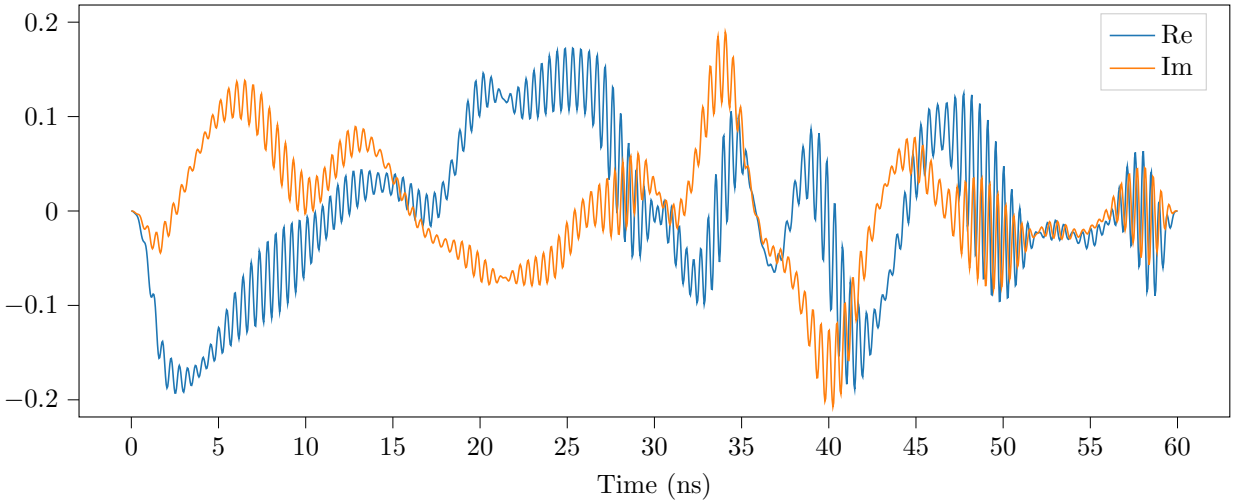

(b) Resonator control pulse shape.

Figure 1.13: Optimized pulse shapes of **(a)** $\Omega_q(t)$ and **(b)** $\Omega_r(t)$. The real and imaginary parts of the pulse are shown in blue and orange respectively. The resonator shows rapid oscillations compared to the qubit.

us information about the the validity of the Hilbert space truncation. In Figure 1.16 the maximum reached occupation probability are plotted for all states. This is done for all the 6 state transfers. Looking only at the odd states there is a clear downward trend for higher states, with $|7\rangle$ only reaching circa 0.2 of occupation probability during the $|0\rangle$ transfer. $|6\rangle$ is in the 0.2–0.3 occupation range for all transfers. The dynamics of the resonator are provided in **??** for further analysis.

Finally we can plot the Wigner function of the final resonator states and compare it with the target states. This is done in Figure 1.17 where the final states have been transformed back into the lab frame. As is evident from the plots they are close to the target states shown in **??**.

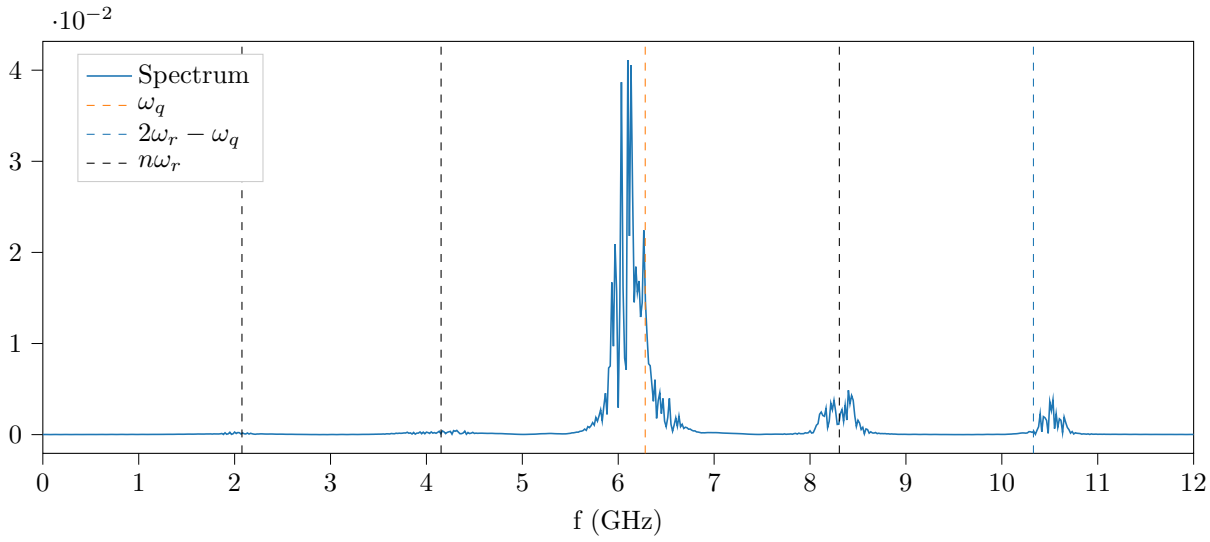

(a) Qubit control pulse spectrum. The black vertical are located at $n\omega_r$ where $n = (0.25, 0.5, 1)$.

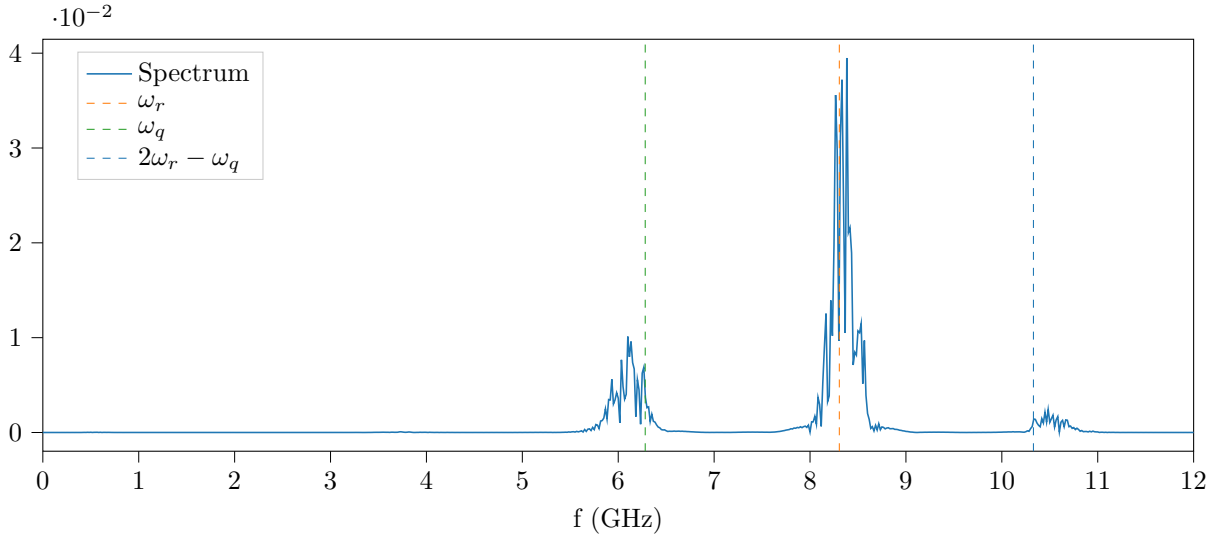

(b) Resonator control pulse spectrum.

Figure 1.14: Spectrum of optimized pulses **(a)** $\Omega_q(t)$ and **(b)** $\Omega_r(t)$ (in the lab frame).

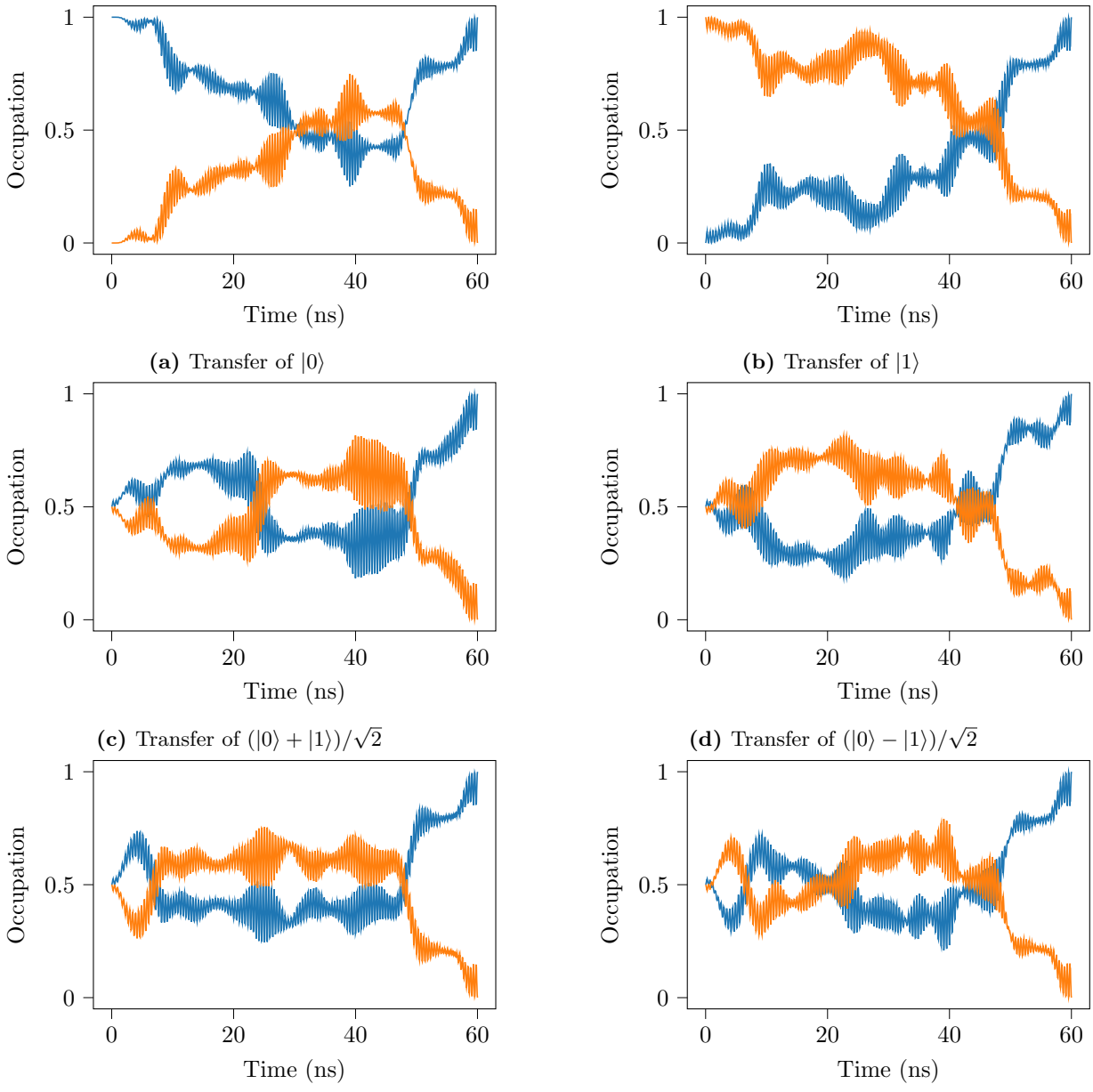

(a) Transfer of $|0\rangle$

(b) Transfer of $|1\rangle$

(c) Transfer of $(|0\rangle + |1\rangle)/\sqrt{2}$

(d) Transfer of $(|0\rangle - |1\rangle)/\sqrt{2}$

(e) Transfer of $(|0\rangle + i\,|1\rangle)/\sqrt{2}$

(f) Transfer of $(|0\rangle - i\,|1\rangle)/\sqrt{2}$

Figure 1.15: Qubit level occupation over time for the 6 state transfers. $|0\rangle$ and $|1\rangle$ are shown in blue and orange respectively.

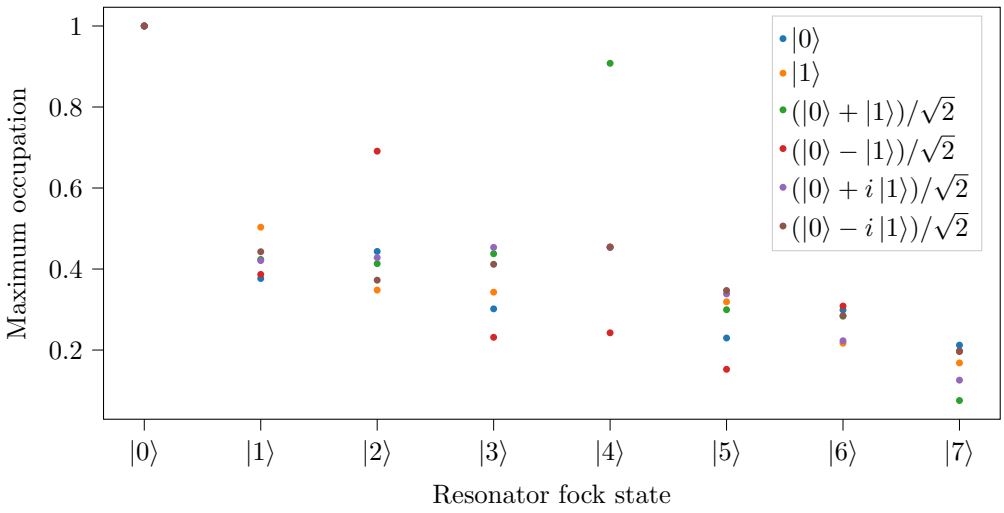

Figure 1.16: asda

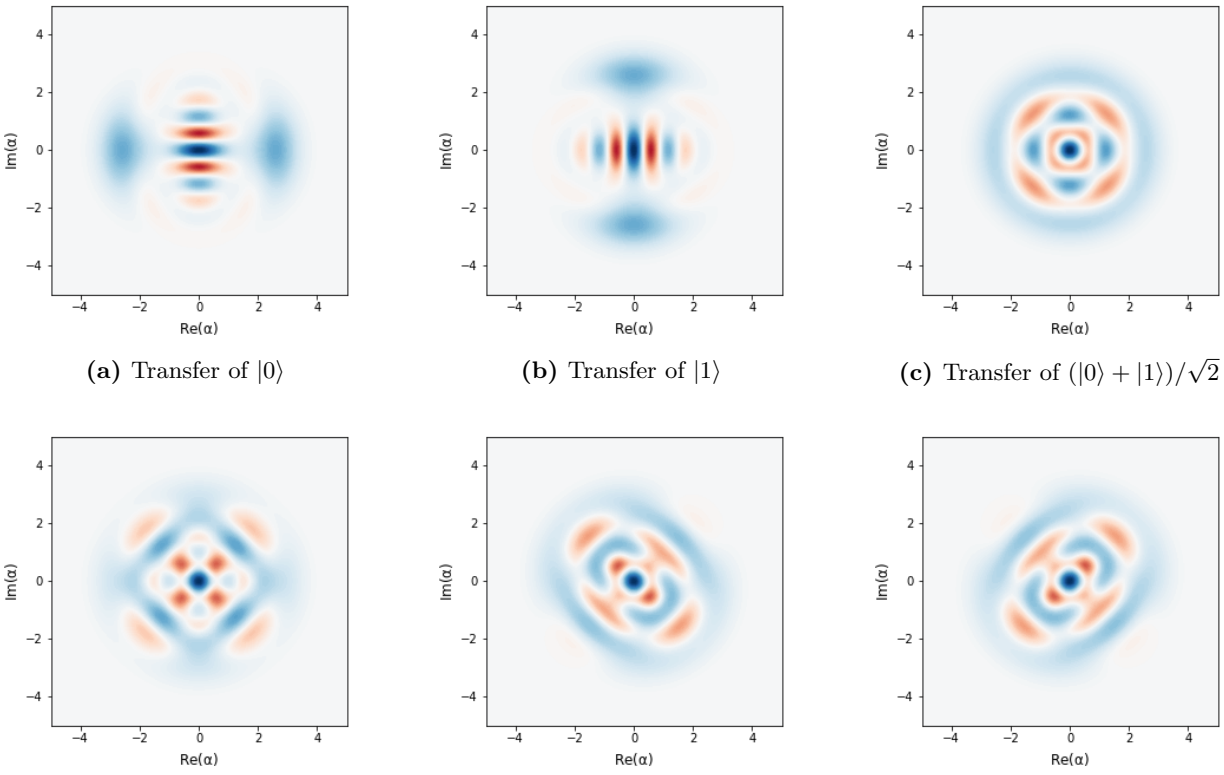

(a) Transfer of $|0\rangle$ **(b)** Transfer of $|1\rangle$ **(c)** Transfer of $(|0\rangle + |1\rangle)/\sqrt{2}$

(d) Transfer of $(|0\rangle - |1\rangle)/\sqrt{2}$ **(e)** Transfer of $(|0\rangle + i\,|1\rangle)/\sqrt{2}$ **(f)** Transfer of $(|0\rangle - i\,|1\rangle)/\sqrt{2}$

Figure 1.17: Wigner function of final state (lab frame) of the resonator for all state transfers. The final resonator states are close to the target states shown in **??**.